Scientific Report

01.12.2015 - 30.09.2017

Project code: PN-RU-TE-2014-4-1444

Project nr. 4/01.09.2015

Project titel**: Functional DNA Nanostructures-Gold Nanoparticles for Targeted Gene Therapy Purposes *(DNAnanoGold)***

Contractor: **"Petru Poni" Institute of Macromolecular Chemistry, Iasi**

Project director: **Dr. Alexandru Rotaru**

http://rotarualexandru.wix.com/dnananogold

Instrument set-up and configuration

For the fulfilling of the current activity, we planned to tune the following available equipment, suitable for the analysis and characterization of both functionalized AuNPs and the prepared DNA-based nanostructures:

- AFM – extensively used for the analyses of AuNPs with different shells, DNA origami nanostructures, DNA-stabilized SWNTs and SWNTs-AuNPs nanocomposites. Specific cantilevers to get best resolutions were utilized (NSG10, NT-MDT) under different scanning conditions in tapping mode (in air and in liquid).
- TEM – extensively used for the analyses of nanomaterials with high contrast in TEM (AuNPs with different shells, DNA-stabilized SWNTs and SWNTs-AuNPs nanocomposites). Specific TEM grids were tested for each material (PURE CARBON FILM 200-400M) to find the best imaging conditions for the specific sample.
- HPLC – used for the characterization of the modified and unmodified DNA sequences. The equipment was adjusted to work under water-buffer-organic solvent system utilizing custom-made HPLC runs to get best separation conditions. Additionally, specific reverse phase HPLC columns used for the analysis of nucleic acids was involved.
- RAMAN – utilized for the characterization of DNA-stabilized SWNTs, SWNTs-AuNPs nanocomposites and for cancer cells SERS imaging.

Purchase, design and modification of the modified DNA sequences

The following modified and unmodified sequences were designed and used for the experiments involving organic fluorescent dye intercalation and corresponding theoretical investigations, theoretical modeling of nucleic acids, functionalization of AuNPs with DNA.

Oligo Name	**Oligo Sequence 5'-….- 3'**
DNA_pack	CAA GCC CTT AAC GAA CTT CAA CGT A
DNA_pack_compliment	TAC GTT GAA GTT CGT TAA GGG CTT G
DNA_Drew_D	CGC GAA TTC GCG
Thiol_15_G	GGG GGG GGG GGG GGG – SH
Thiol_25_G	GGG GGG GGG GGG GGG GGG GGG GGG G – SH
Thiol_40T	TTT TTT TTT TTT TTT TTT TTT TTT TTT TTT TTT TTT TTT T – SH
Thiol_5T_NH2	NH2 – TTTTT – SH
TAMRA_40_A	AAA AAA AAA AAA AAA AAA AAA AAA AAA AAA AAA AAA AAA A – TAMRA
Thiol_15_G	GGG GGG GGG GGG GGG – SH
Thiol_25_G	GGG GGG GGG GGG GGG GGG GGG GGG G – SH
t3s6e_amino_5	NH2 – TTTCACCGGAAAGCGCGTTTTCATCGGAAGGGCGA
t3s4e_amino_3	TGTACTGGAAATCCTCATTAAAGCAGAGCCACTTT – NH2
t4s5f_amino_5	TTTCTCAGAGCATATTCACAAACAAATTAATAAGT – NH2
TAMRA_40_C	TAMRA – CCC CCC CCC CCC CCC CCC CCC CCC CCC CCC CCC CCC C

Synthesis, functionalization and testing of the AuNPs.

Synthesis of AuNPs functionalized with cationic polymer

In order to induce the interaction of nucleic acids with gold nanoparticles (AuNPs), we investigated the synthesis of AuNPs involving polyethylene imine (PEI, Mr = 15.000 Da) as a templating cationic polymer. Numerous ratios of $HAuCl_4$ and PEI have been tested during this step of the project, including variation of concentration of the reaction components, keeping the concentration of $HAuCl_4$ constant and varied the amount of PEI in the reaction mixture, keeping the PEI concentration constant and varying the $HAuCl_4$ concentration, or using keeping both components at same ratio, but varying their concomitant concentration in the reaction mixture. Interestingly, the reaction mechanism was different when testing the above mentioned condition (Fig. 1).

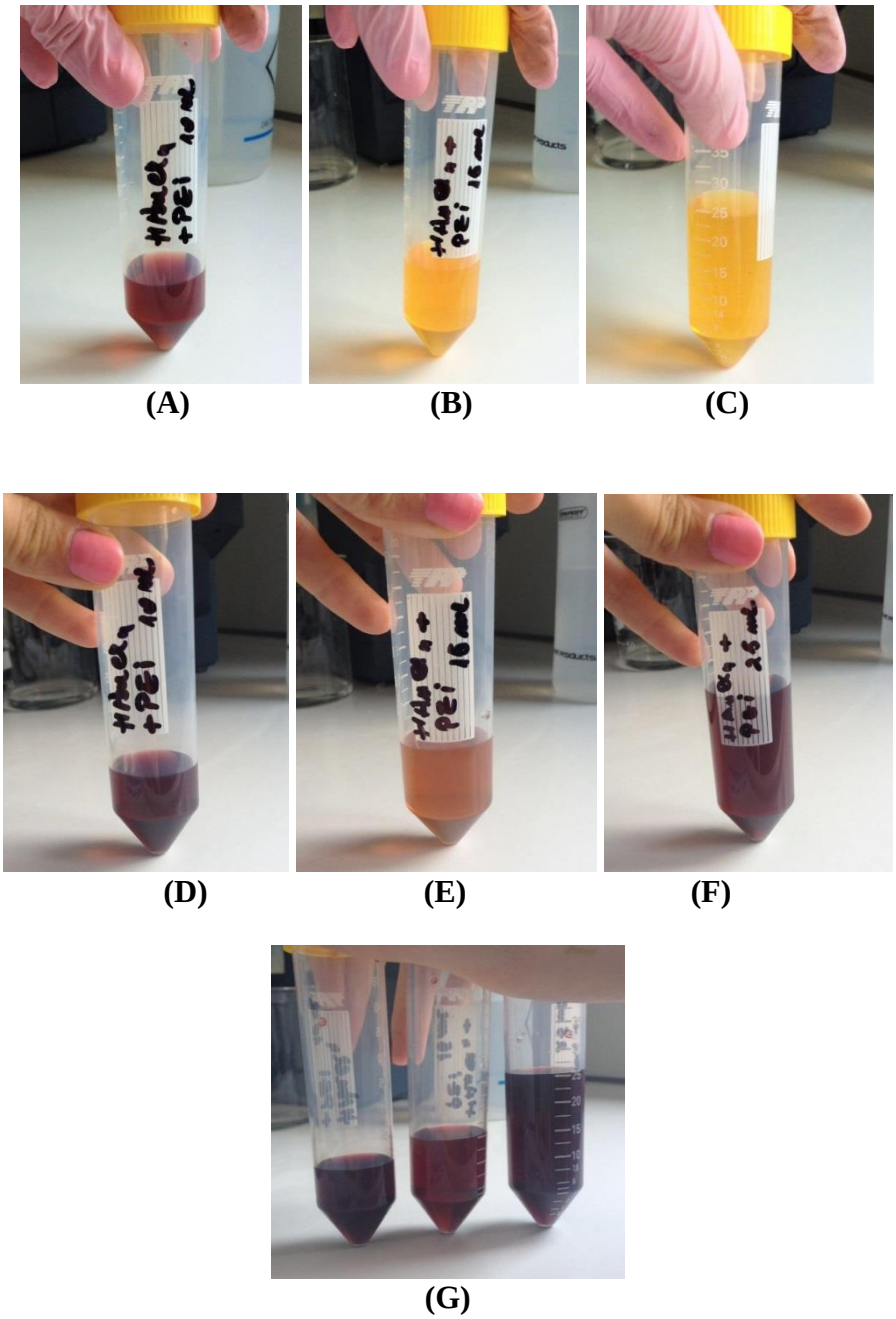

Figure 1. Pictures of reaction mixtures for AuNPs preparation at different reaction times.

Analyzing the Dynamic Light Scattering (DLS) results, we could observe that Zeta potentials of all investigated sample are positive, meaning that the prepared AuNPs possess a shell of the PEI. Also, DLS data suggested an approximate size of the investigated samples, the determined dimensions varied from 7 to 12 nm. The TEM analysis revealed indeed presence of more or less uniform AuNPs of a 10 nm and sub 10 nm in size, data similar to the DLC analysis (Fig. 2).

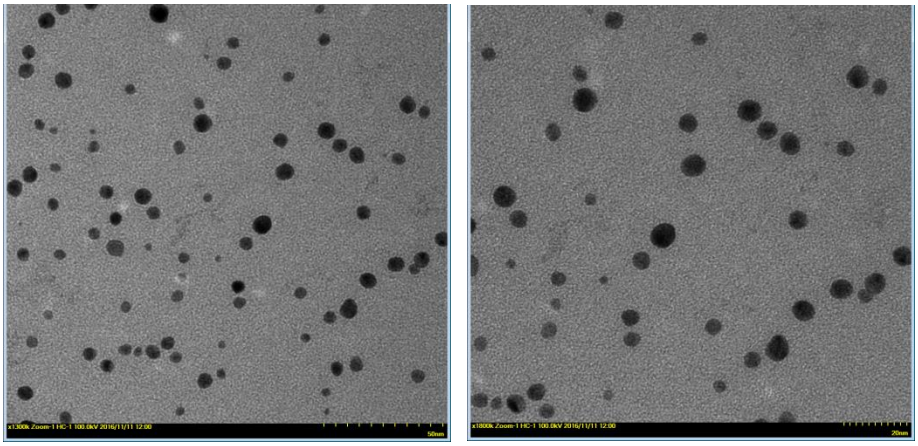

Figure 2. TEM analyses of AuNPs-PEI; scale bar – 50 nm (left), scale bar – 20 nm (right).

Another successful experiment was performed when varying only the concentration of $HAuCl_4$ while keeping the concentration of PEI constant (Fig. 3).

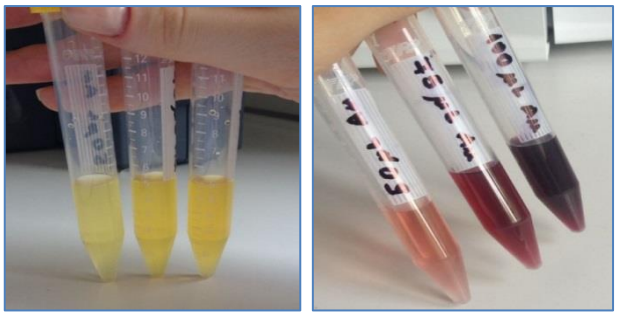

(A) **(B)**

Figure 3. Pictures of reaction mixtures at different concentrations.

Additional information was obtained by careful analysis of multiple TEM images (Fig. 4). We could observe huge agglomerations in some areas on the TEM grid (Fig. 4 left).

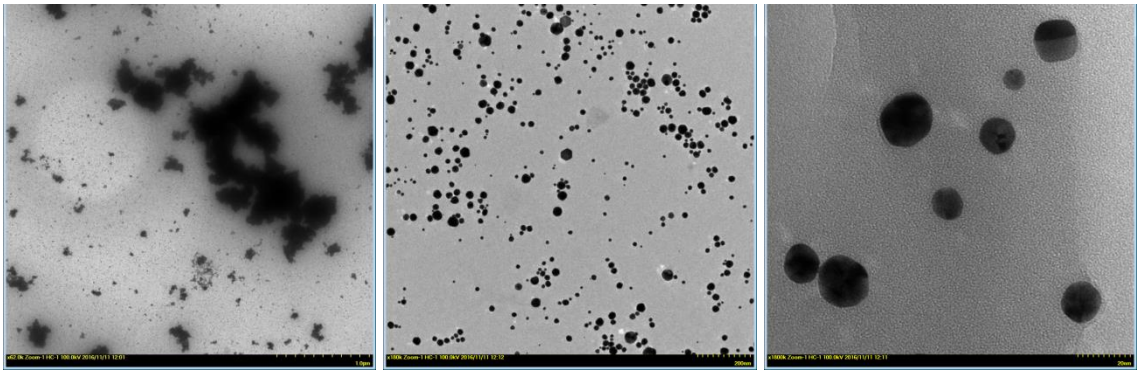

Figure 4. TEM analyses of samples; scale bar – 1 um (left), scale bar – 200 nm (middle), scale bar – 20 nm (right)

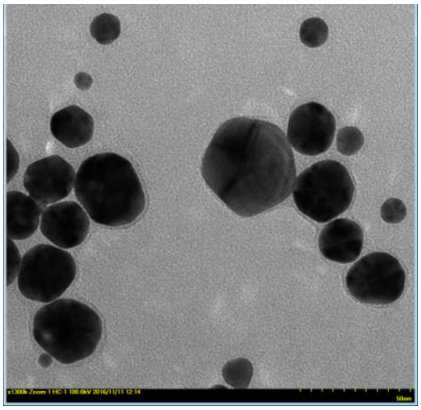

Besides the large agglomerations, nanoparticles of different sizes ranging from 10 to 30 nm were also observed (Fig. 4 middle, right). The observed agglomerations could be explained after careful analysis of individual small AuNPs. In several TEM pictures AuNPs possess an evident shell around nanoparticle (Fig. 5).

Figure 5. TEM analysis, scale bar – 50 nm.

In conclusion, at this step of the project we succeeded to find optimum conditions for the preparation of AuNPs with a cationic shell able to compact nucleic acids. Importantly, we found conditions for the preparation of small 10 or sub-10 nm AuNPs as well as larger AuNPs.

Preparation of cyclodextrin-functionalized AuNPs.

The overall strategy for the preparation of the cyclodextrin-functionalized AuNPs (CD-AuNPs) includes several synthetic steps. First, bare phosphine-stabilized AuNPs are covered with amino-modified synthetic DNA (Fig. 6). The thiol group in the designed short synthetic DNA strand (NH_2-TTTTT – SH) ensures the affinity towards the AuNPs.

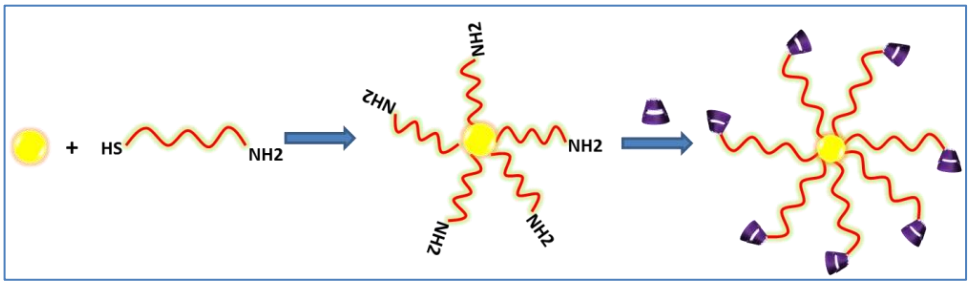

Figure 6. Schematic representation of the reaction step for the preparation of amino-functionalized AuNPs.

Thus obtained amino-modified AuNPs are purified, characterized and used in the next step for the reaction with the synthesized cyclodextrin mono-modified isothiocyanate (scheme 1).

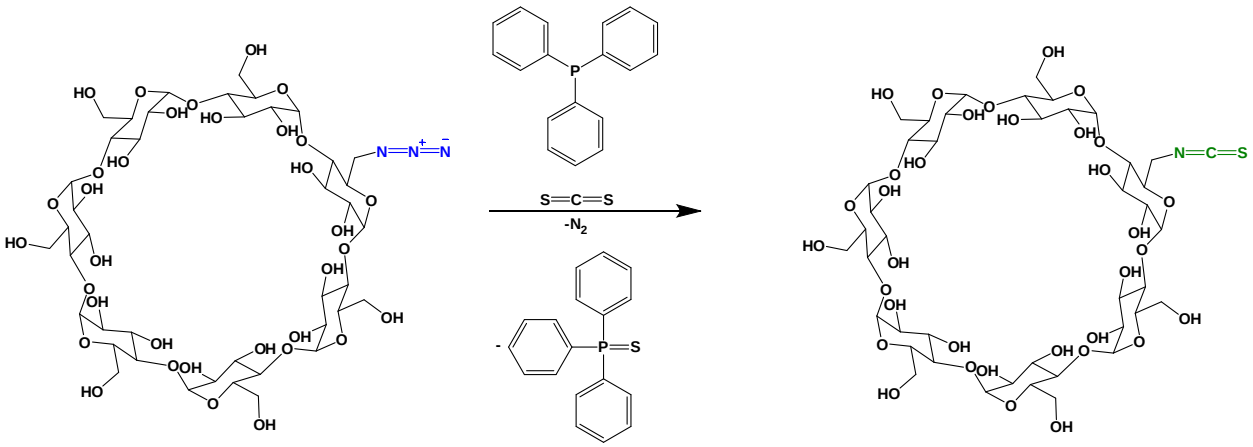

Scheme 1. Synthesis of mono-6-isothiocyanate-6-deoxy-β-cyclodextrin.

The freshly prepared mono-6-isothiocyanate-6-deoxy-β-cyclodextrin was reacted together with the DNA amino-modified gold nanoparticles to yield the final gold nanoparticle with β-cyclodextrin shell according to Fig.6. Transmission Electron Microscopy (TEM), Fourier Transformed Infrared Spectroscopy FT-IR, mass spectrometry ESI-MS and zeta potential measurements were utilized to characterize the final AuNPs-CD.

DLS Zeta potential data of the investigated reaction was crucial at this step, we were following all changes at each step of the synthesis (Table 1).

Sample	Zeta potential (mV)
AuNP-phosphine	-16.53
AuNP-5T-NH2	-20.71
AuNP-5T-CD	-21.58

Table 1. Zeta potential for the starting AuNPs, intermediate amino-modified AuNPs and final AuNPs-CD.

After the attachment of the amino-thiol-modified DNA sequence, the Zeta potential of the product changed from -16.53 for phosphine-coated AuNPs to -20.71. The attachment of the cyclodextrin moiety to the AuNPs further increased the negative value of the AuNPs to the -21.58, proving the attachment of the cyclodextrin by the formation of a thiourea bond.

The obtained functionalized nanoparticles are suitable for the preparation of supramolecular assemblies and afford the possibility to form inclusion complexes with the desired molecules for subsequent biomedical applications.

Assembly and AFM imaging of complex DNA origami nanostructures.

The next step of the project was the assembly of various DNA-based nanostructures. First, we established several protocols for the thermal annealing of the complex DNA origami nanostructures. We have prepared several annealing programs with different speed of cooling to 10^0C. Three different programs were chosen: 4 hours, 12 hours and overnight program. Next, we tuned the AFM equipment in order to be able to measure the nanostructures whose overall size represented a triangle (120x120x120) nm with the theoretical height of 2 nm. Finally, we started to obtain suitable AFM

pictures that showed the desired DNA triangles on the mica surface when scanning in air (Fig. 7). Still, as it could be observed from taken pictures, the agglomeration problem is not entirely solved, the nanostructures tend to stick to each other during the deposition and drying of the sample on the mica surface. Large areas of agglomerations are still present, but with the much better resolution.

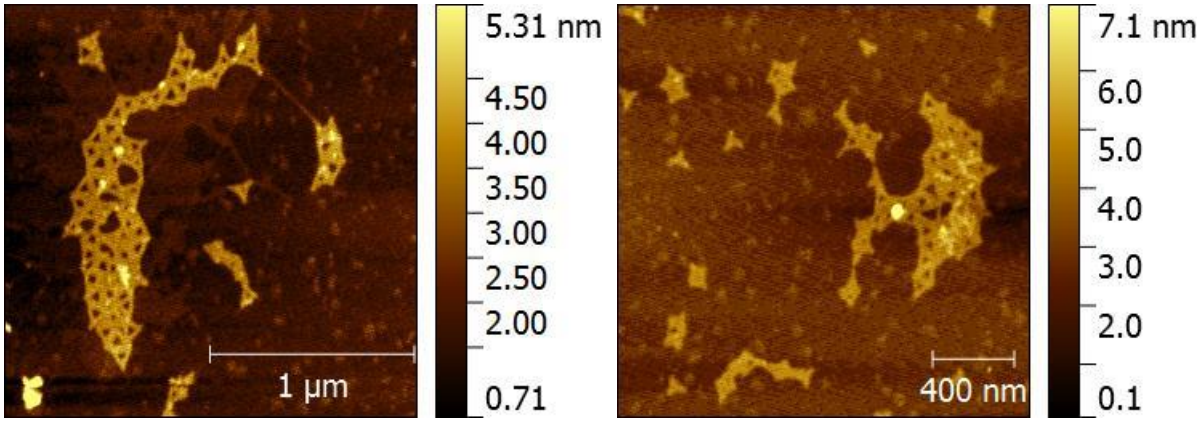

Figure 7. Successful AFM images of DNA origami triangle nanostructure in different conditions.

In conclusion to this research activity, the optimum condition for the preparation and AFM imaging of very complex DNA nanostructures is still under investigation. In the next part of the project we will focus on using different types of AFM cantilevers to get better resolution on complex DNA nanostructures in order to be able to visualize the introduction of the AuNPs to their surface through the cyclodextrin inclusion complex formation.

Assembly of simple DNA assisted nanostructures.

We continued the topic on preparation of the DNA nanostructures by simplifying the design of the final assembly. The proposed design was based on the DNA functionalized AuNPs, prepared in previous project activities, and single-walled carbon nanotube (Fig. 8).

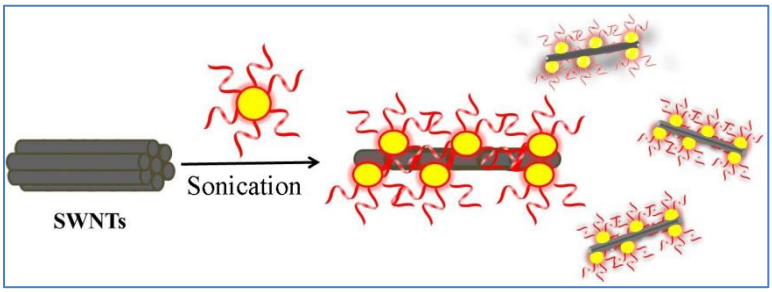

Figure 8. Proposed synthetic pathway for the preparation of water-soluble SWNT-AuNPs nanocomposites starting from the DNA-functionalized gold nanoparticles and pristine single-walled carbon nanotubes.

Singe-walled carbon nanotubes (SWNTs), have attracted significant interest in the area of bio-oriented medicine, for potential applications in biological detection, drug delivery, phototherapies, and biomedical imaging.

Optimization of SWNT-AuNPs preparation

The obtained DNA-functionalized AuNPs (AuNPs-DNA) were used for the functionalization of SWNTs. Raw SWNTs were mixed together with a fixed amount of AuNPs-DNA in 1xTAE buffer and sonicated in a conventional VWR ultrasonic bath. Aliquots from the reaction mixture were collected

every 30 min and the Raman signal enhancement by measuring the spectra under 633 nm laser excitation was monitored. Particularly, the G-band peak at ~1590 cm-1 was observed, being the most intense Raman feature of SWNTs and can be used as a direct measure for the SWNT distribution inside the biological samples.

The reaction mixture after 60 min of sonication was analyzed by AFM and TEM analysis, proving the attachment of AuNPs to the SWNTs.

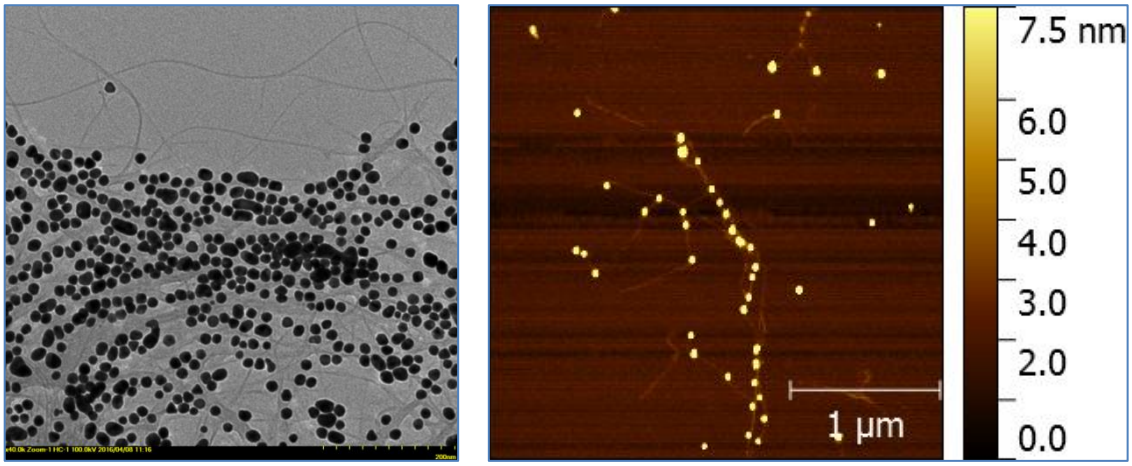

Figure 9. Examples of TEM and AFM images taken for samples after 60 minutes of sonication containing 5 µL SWNTs; scale bar – 200 nm (left) and 100 nm (right). Low contrast SWNTs were observed in all of

In conclusion to this research activity, a DNA-assisted method has been developed to decorate gold nanoparticles onto pristine SWNTs in the solution phase, yielding SWNT-AuNPs nanocomposites which exhibited noticeable SERS effect. The synthetic pathway is established in such manner that, by choosing the right dimensions of the commercial or custom made citrate coated AuNPs in the first step, it is possible to have the desired size AuNPs in the final SWNT-AuNPs nanocomposite. Moreover, the developed methodology for the preparation of SWNT-AuNPs nanocomposites took into account the possibility of post-synthetic functionalization through complementary hybridization with molecules of interest attached to a complementary DNA strand using well-developed bio-conjugation chemistry. This post-synthetic hybridization possibility was verified by monitoring the quenching of fluorescence signal of TAMRA fluorophore-labeled complementary DNA strand.

The resulted SWNT-AuNPs represent an interesting nanoplatform with easy to tune size of AuNPs and facile decoration with large library of small molecules known or easy to attach to synthetic DNA. These make the final nanocomposites promising candidates in selective cancer cell labeling and imaging, nanoscale electronics or sensor developments. Further research towards the increasing the density of AuNPs within the SWNT-AuNPs nanocomposites, possibility of nanocomposite positioning (immobilization) on various surfaces through hybridization or construction of even more complex nanostructures due to available hybridization binding sites are under investigation in our group.

Transfection experiments and RAMAN imaging of HeLa cancer cells using SWNT-AuNPs

Cell toxicity test was carried out first to determine the cytotoxicity of the synthesized SWNT-AuNPs nanocomposites at optimum conditions prior to cell transfection experiments. Cytotoxicity was measured using the CellTiter 96® Aqueous One Solution Cell Proliferation Assay (Promega) following manufacturer protocol. HeLa cells were seeded at a density of 10^4 cells per well in 96 well plates, in complete medium. The next day, cells were treated with the freshly-prepared SWNT-AuNPs reaction mixture and then grown for another 24 hours. Next, 20 µL of CellTiter 96® Aqueous One Solution reagent were added to each well, and the plates were incubated for another 4 hours before reading the result. Absorbance at 490 nm was recorded with a plate reader (EnSight, PerkinElmer). Cell viability was calculated and expressed as percentage relative to viability of untreated cells. Experiments were performed in two duplicates and repeated two times. Data is presented as mean±S.D. (n=4). The obtained experimental results revealed a cell viability higher than 75% at all tested concentrations (Fig. 10).

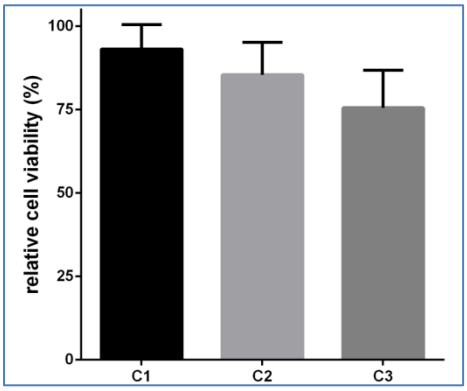

Figure 10. In vitro cellular toxicity assay: relative cell viability of HeLa cells.

Next, HeLa cells were incubated with freshly prepared SWNT-AuNPs for 24 hours, washed extensively with ultrapure water and afterwards fixed with 2.5% glutaraldehyde prior to Raman imaging. Twenty four hours prior transfection, HeLa cells were plated in chamber slides with 8 wells (Lab Tek) at a density of 10^4 cells/well and allowed to attach overnight. Cells were treated with the freshly-prepared SWNT-AuNPs reaction mixture (5 µL of SWNT-AuNPs in 200 µL of medium) and after 24 hours, they were fixed with 2.5% glutaraldehyde for 15 minutes and imaged under a Raman confocal microscope (inVia, Renishaw) with a 633 nm laser (17 mW) as the excitation light source. A 50× objective lens was used and each Raman spectroscopic map contained at least 90 × 90 spectra, with 1 s integration time for each spectrum (Fig. 11). The imaging was conducted using a 633 nm laser (17 mW) as the excitation light source. Additionally, an optical microscope equipped with 50× objective lens was used to compare the optical and Raman image of the investigated area.

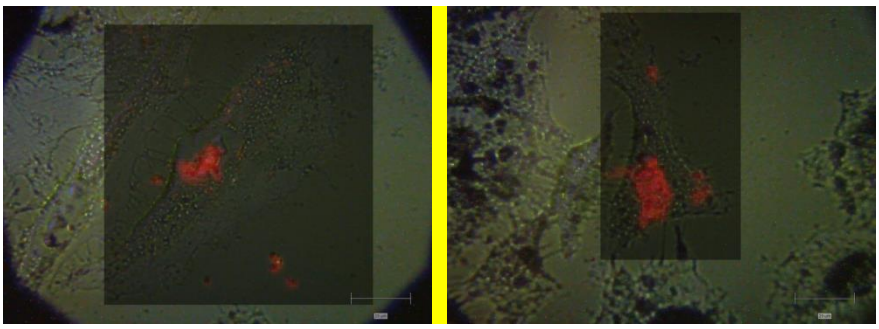

Figure 11. Examples of overlapped optical and Raman images of HeLa cancer cells incubated with AuNPs-CNT for 24 hours at 37°C.

Under these experimental conditions, strong Raman signals were observed and, the recorded red areas in the Fig. 11 corresponded to G-band intensities that can be used as an indicator of the SWNT-AuNPs composites presence in the analysed cells. By overlapping optical and Raman images (Fig. 11) we could note that red areas were predominantly located on the HeLa cells, with little or no background signals observed in the analysed images, showing the specific attachment of SWNT-AuNPs to cells.

Assembling DNA-based nanostructures with modifications capable of forming inclusion complexes with cyclodextrin.

The complex DNA-based nanostructures functionalized with prepared in previous Activities were used as a support for the positioning of the cyclodextrin-functionalized AuNPs. Thus, the mixture of sequences necessary for assembling the nanostructure was subjected to thermal treatment (anealing) resulting in the assembly of nanostructured "triangles". The resulting mixture was subjected to AFM analysis to visualize the formation of correct nanostructures (Fig. 12).

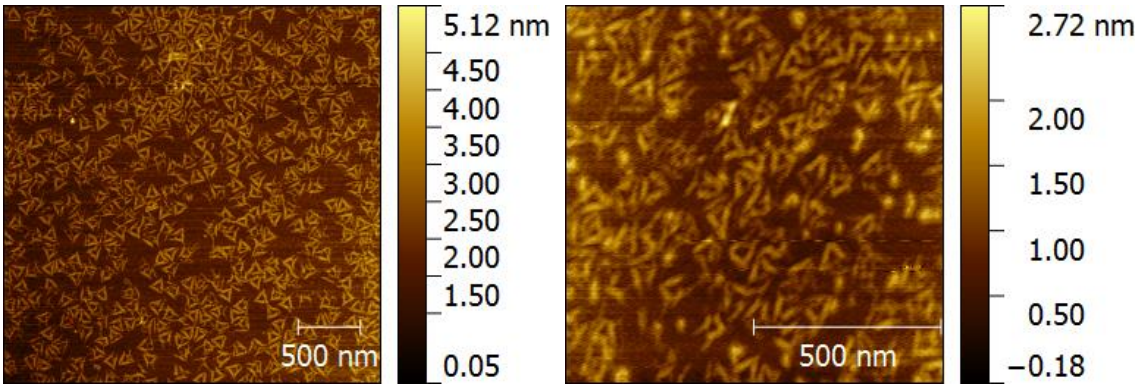

Figure 12. AFM images of DNA-based nanostructures with biotin surface modifications.

AFM analysis showed correct assembly of nanostructures as triangles (Fig. 12, (left)). Because of the small size of the Biotin molecules, these modifications can not be seen by AFM, and their presence is determined indirectly.

Surprisingly, the destruction of nanostructures was observed at a higher magnification (Fig. 12 right), on the small scale we could see assembled nanostructures as well as fragments of final structures. The destruction of nanostructures on the small scale scanning was confirmed by measuring a large number of samples, the phenomenon observed at each measurement. This could negatively influence the visualization of any modification on the surface of the nanostructures because attaching gold nanoparticles to the surface of the nanostructure is done by supramolecular interactions that are much weaker than covalent bonds.

Positioning of AuNPs-CD on the surface of DNA nanostructures by forming the cyclodextrin inclusion complex.

The "triangle" DNA nanostructures deposited on the mica surface were treated with the cyclodextrin functionalized AuNPs (AuNPs-CD) to form an inclusion complex on the surface of the nanostructure (Fig. 13).

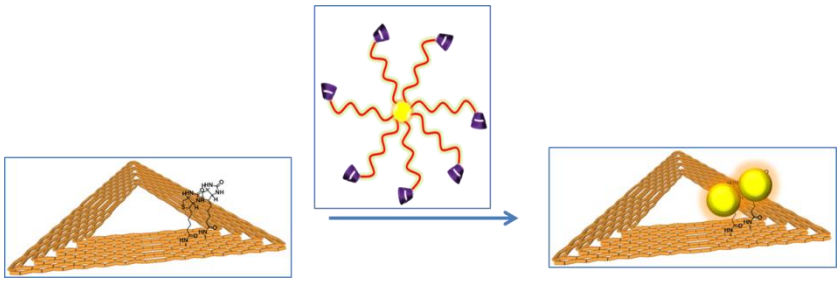

Figure 13. Schematic representation for attaching AuNPs-CD to an origami DNA nanostructure by host-host interaction.

The analysis mixture was allowed to dry and the mica surface was then washed three times with distilled water, dried and subjected to AFM analysis. Analyzing the mica surface after attachment of AuNPs-CD we noticed the decrease of the number of nanostructures attached to the small, which is explained by repeated washing of the surface with water (Fig. 14).

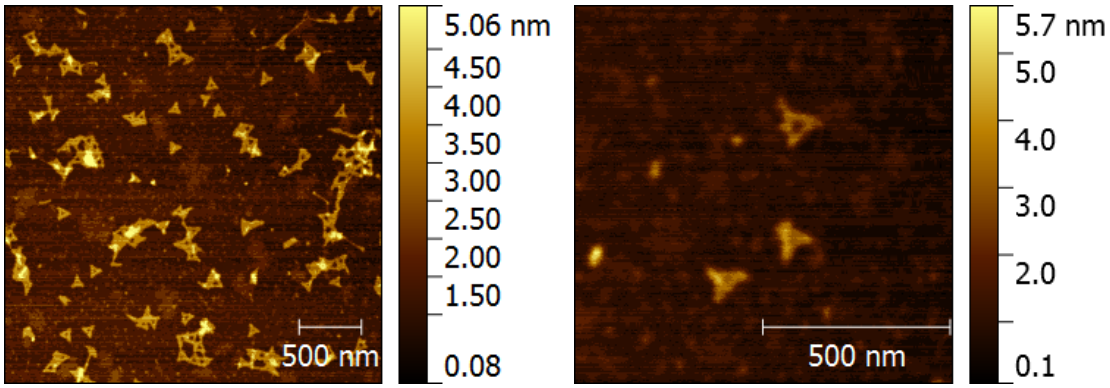

Figure 14. AFM images of DNA nanostructures after treatment with the AuNPs-CD solution.

Also, some of the nanostructures appear with an elevation on their surface, which could prove the attachment of the AuNPs-CD to the surface of DNA nanostructures. At higher magnification (Fig. 14

right) these elevators could not be observed due to the decrease in the resolution of the obtained images.

To obtain a better resolution, the experiment was repeated, and the sample was visualized with AFM in the liquid mode (Fig. 15).

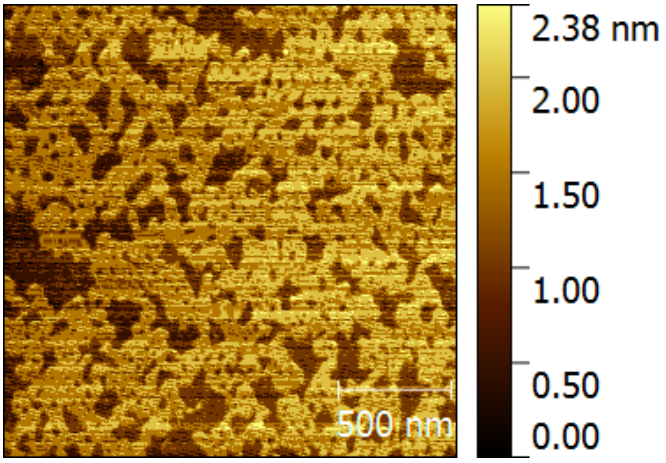

Figure 15. AFM images of DNA nanostructures after treatment with the AuNPs-CD solution and visualized in liquid mode.

Although the data from the literature shows that DNA-based nanostructures are viewed at a much better resolution than in the air, in our case the many experiments with DNA nanostructure solutions have shown unsatisfactory results. It was not possible to visualize not only the modifications on nanostructured surfaces, but it was difficult to identify the joining of structures in the triangular shape.

In vitro investigations of supramolecular assemblies based on host-host inclusion complexes of cyclodextrin.

To verify the behavior and toxicity of inclusion complexes of cyclodextrin with various compounds, we synthesized, complexed and tested a fluorescent compound that possessed increased toxicity. Thus, fluorescence pyridinium indolysin **4** salt (Scheme 2) was conceived as a potentially pH-sensitive dye and synthesized with moderate yield by a two step method based on our previous knowledge in the preparation of substituted idolizines.

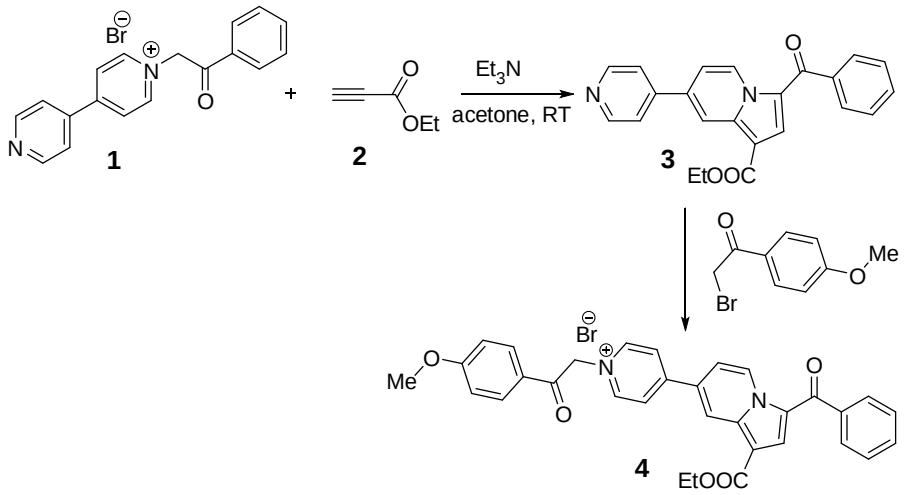

Scheme 2. Synthesis of pyridinium indolizine salt **4**. Compounds 1 and 3 have been reported previously.

Due to the presence of the pyridinium group in compound **4**, the appropriate nitrogen ilyde may be formed in the presence of a base according to scheme 2. This reversible property influences the emission spectrum, making it a pH-sensitive fluorescent dye.

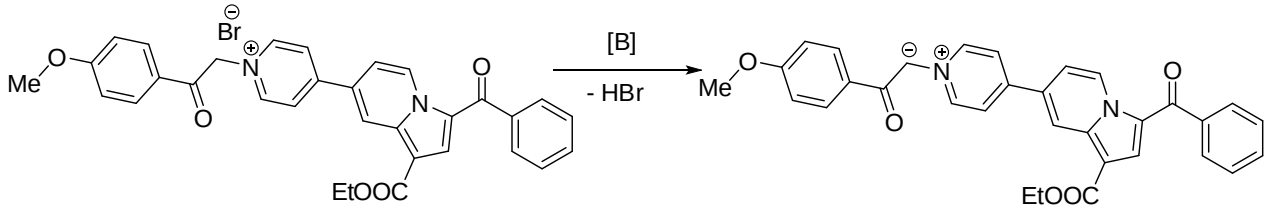

Scheme 3. General presentation of the ilyde formation of the compound **4**.

The applications of these compounds are limited due to problems connected to water solubility, compound **4** has a partial solubility in DMSO and dichloromethane. In order to obtain a better water solubility of compound **4** and to extend its applications as cell marker or cell-sensitive dye, we proposed to synthesize a formulation between compound **4** and β-cyclodextrin (β-CD). To this end, pyridinium indolysin **4** salt was suspended in water and then different amounts of β-CD corresponding to the following equivalent ratios of compound **4** to β-CD 1:1; 1:1.5; 1:2; 1:3) were carefully added. The mixtures were heated to 110 ° C to ensure the solubility of the added cyclodextrin and to facilitate the solubilization of compound **4** by β-CD interaction. The solution was allowed to cool slowly at room temperature and it was observed that starting with a ratio of 1:1.5, after cooling, the reaction mixture became transparent, with a little precipitate or not at all. This observation suggests that the solubilization of compound **4** is determined by the possible formation of the host-host inclusion complex. Interestingly, at the 1:1 ratio, the solution after the cooler was still cloudy suggesting the incomplete solubilization of compound **4**, and we can conclude that large amounts of β-CD are needed to stabilize the complex. On the other hand, higher ratios could lead to the formation of supramolecular assemblies containing inclusion complexes consisting of a compound of molecule **4** and two or more

β-CD units. To verify this hypothesis, ESI-MS measurements were made for reaction mixtures with different ratios between Compound 4 and β-CD (1:1.5; 1:2 and 1:3). ESI-MS is a fast and simple method for the study of inclusion phenomena that allows for rapid determination of CD stoichiometry: guest. The ESI-MS spectra (Fig. 16) for the 1:1.5 ratio clearly show the presence of several bands corresponding to compound **4** (519-M + -Br), β-CD (1157- M + CD (1654-M + -Br + CD) and complex 1:2 compound **4**:β-CD (2788.83 - M + -Br + 2CD).

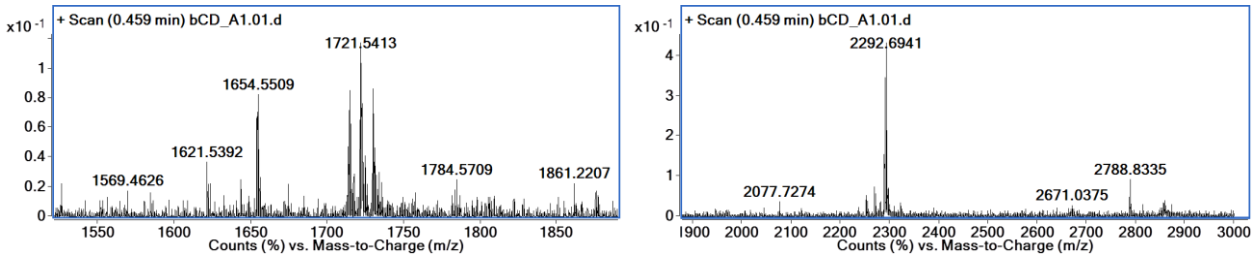

Figure 16. The ESI-MS spectra of the mixtures between compound **4** and β-CD for the ratio of 1:1.5 can be seen in the presence of several bands corresponding to the inclusion of the 1:1 inclusion complex (1654-M + -Br + CD) and compound 1:2 compound 4: β-CD (2788.83 - M + -Br + 2CD).

For all analyzed samples the formation of host-host inclusion complex was observed. Interestingly, the corresponding bands for both 1:1 and 1:2 complexes (M + -Br + CD and M + -Br + 2CD) can still be observed with increasing stoichiometry between host and guest (ratio 3:1). However, adding an excess of cyclodextrin in order to ensure the formation and observation of only the multi-cyclodextrin ions did not lead to a single species, both species 1:1 and 1:2 being present in the reaction mixture. The structural foundations for the formation of these species were verified by molecular docking simulations.

In vitro cell viability studies (MTS assay)

Prior to performing cell staining experiments, the cytotoxicity of compound **4** and its inclusion complex **4_CD** was studied on two cell lines: one human cancer and one human normal (HeLa and NHDF). Cytotoxicity, measured as inhibition of cell line viability, was assessed at 48 h of incubation (Fig. 16). Analyzing the data obtained, compound **4** showed very high toxicity values for all five investigated concentrations (0% cell viability) on the HeLa cell line (Fig. 16, (left)) and high (for concentrations: 34.8 μM; 52.2 μM, 69.6 μM and 86.9 μM) to medium toxicity (for a concentration equal to 17.4 μM) on NHDF cells (Fig. 16, (right)).

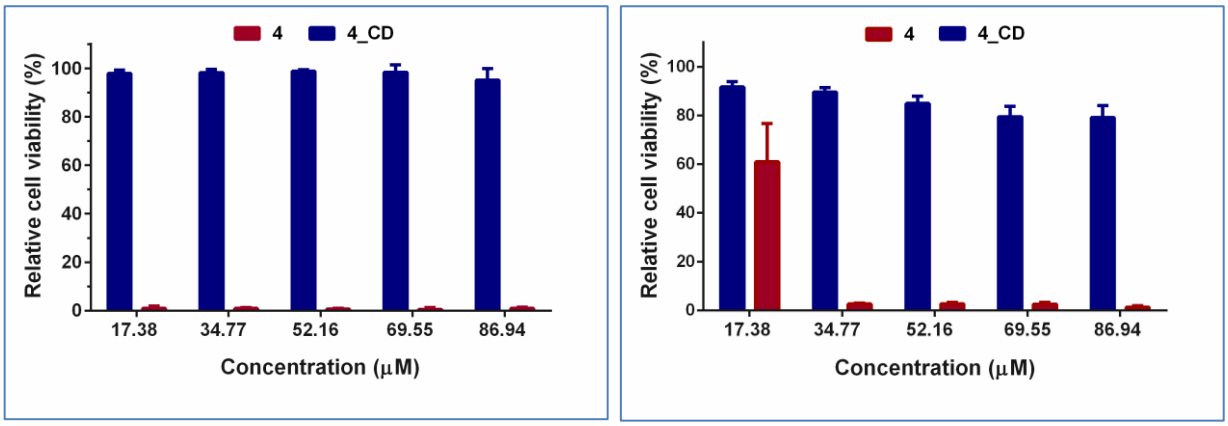

Figure 16. *In vitro* cell viability (MTS assay) for compound 4 and 4_CD for HeLa (left) and NHDF (right) cell lines.

Analyzing data on the cell viability of complex **4_CD** with the same concentrations of compound **4**, we observed surprisingly high (over 95%) cell viability for all HeLa cells studied (Fig.16, (left)) and values (over 80%) of cell viability with a slight decrease in the concentration of inclusion complex in NHDF cells (Fig. 16, (right)).

In vitro cell imaging experiments

Two cell lines (HeLa) and (NHDF)) were used to characterize the ability of the **4_CD** complex to be used as a dye for living cells. For this purpose, five solutions of different concentrations (17.4 μM; 34.8 μM; 52.2 μM; 69.6 μM and 86.9 μM) of compound **4_CD** were added to the two cell lines investigated; the wells were visualized simultaneously after 15 minutes and 24 hours using a Leica DMI 3000 B inverted microscope with a GFP fluorescence filter. The comparative images for HeLa and NHDF after assimilation of compound **4_CD** at 15 minutes and 24 hours are shown in Fig. 17. The distribution of compound **4_CD** for both cell lines looks similar after a 15 minute incubation time for all concentrations studied, indicating a uniform extranuclear location (Fig.17, (left)).

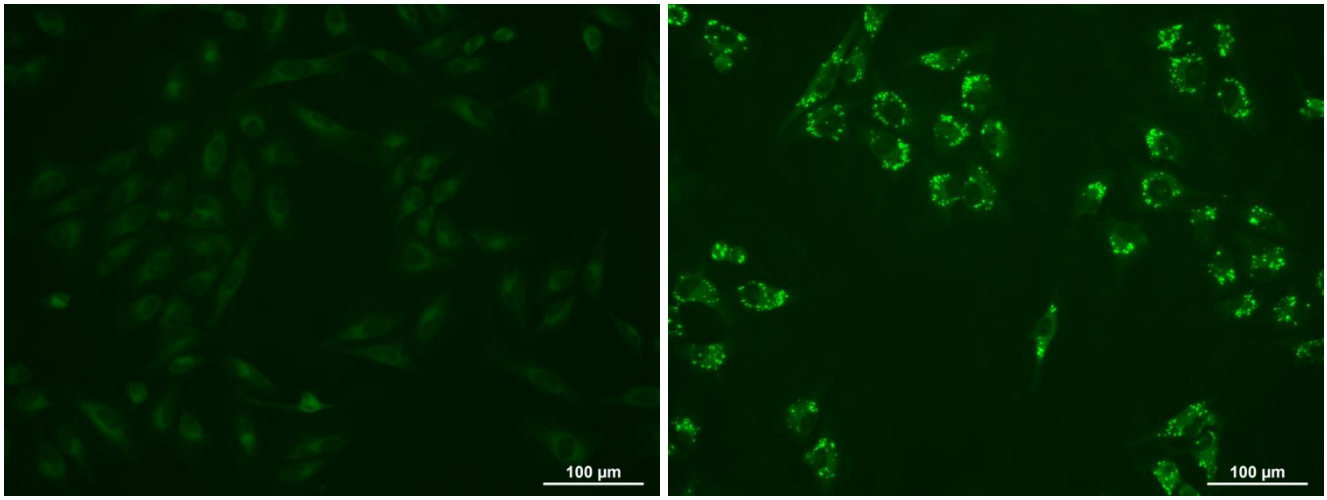

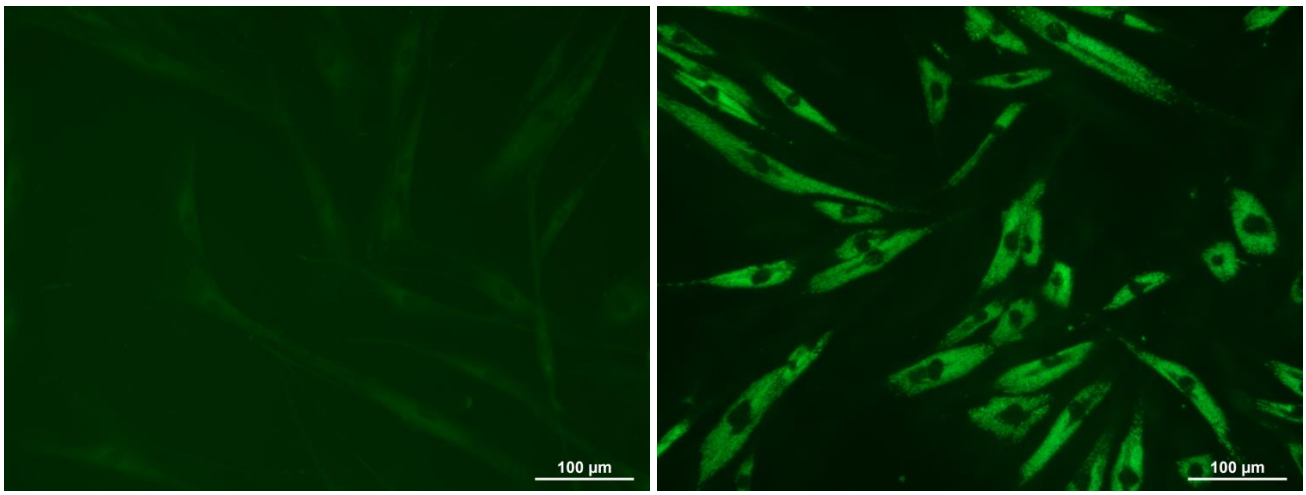

Figure 17. Assimilation of compound **4_CD** in HeLa (up) and NHDF (bottom) cells after incubation time of 15 min (left) and 24 h (right).

The image changes dramatically after 24 hours of incubation, the extranuclear location of the dye was still observed, but with clear accumulations in the cytoplasm (Fig.17, (right)). In addition, a general increase in luminosity was observed when comparing images after 15 minutes and 24 hours at the same concentration of **4_CD**. Interestingly, as with NHDF cells, accumulations in the cytoplasm are smaller and more uniform than those observed for HeLa cells. The large and localized **4_CD** accumulations in HeLa cells indicated a specific interaction of the dye with certain cellular components. Considering the nature of the **4_CD** complex and its property of having a higher fluorescence intensity at a lower pH, we can assume that dye accumulation takes place preferentially in acidic cell organelles. In order to verify this hypothesis, a co-staining experiment was performed using LysoTracker Red DND-99, a commercial agent used to color acidic cell organisms.27,28 Thus, HeLa cells stained with **4-CD** for 24 hours were treated followed by 75nM LysoTracker Red DND-99 (Invitrogen) for 30 minutes at 37 ° C in 5% CO2. The cells were then washed 3 times in PBS and visualized in fresh culture medium using a Leica DMI 3000 B reversed microscope equipped with GFP and N2.1 filters (Fig.18, (left) and (middle)).

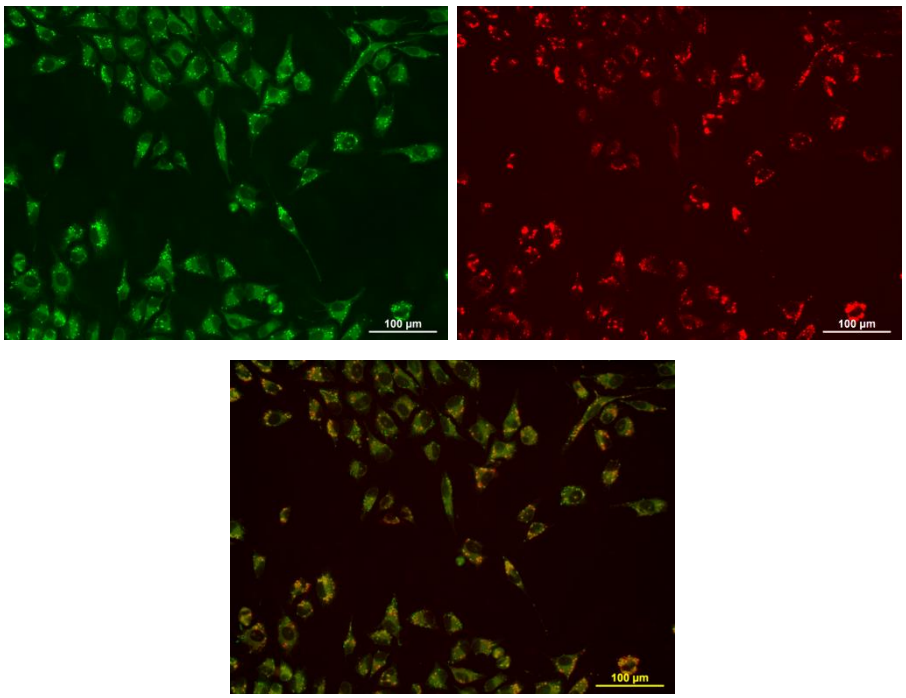

Figure 18. Assimilation and distribution in HeLa cells: left-**4_CD** after 24 h; middle -LysoTracker Red DND-99 after 30 min (filter N2.1); right - images overlapped for those filters (GFP and N2.1).

By overlaying colored images with **4_CD** and LysoTracker Red DND-99 (Fig. 18, (right)), a similar accumulation for both staining agents in the same regions of studied HeLa cells was observed. The obtained results support the initial assumption of specific accumulations in acidic cell organelles.

Dissimination

List of published and submitted publications:

1. G. Pricope, M. Serdaru, E. L. Ursu, C. Cojocaru, L. Clima, N. Marangoci, R. Danac, I. Mangalagiu, M. Pinteala, A. Rotaru*. Novel pH-sensitive Supramolecular host-guest assembly for staining cell acidic organelles. *Polymer Chemistry*. Sent for publication, manuscript ID: PY-ART-09-2017-001668 (2017).

2. T. Vasiliu, A. Dascalu, M. Pinteala, C. Cojocaru, A. Rotaru*. Polyplex formation between cyclodextrin-based non-viral vector and dsDNA: molecular dynamic study with experimental validation. *Revue Romain de Chimie*, Sent for publication, manuscript ID: RRC 1187 (2017).

3. A. Rotaru, G. Pricope, T. Planck, L. Clima, E. L. Ursu, M. Pinteala, J. Davis, M. Barboiu. G-Quartet Hydrogels for Effective Cell Growth Applications. *Chemical Communications.* Sent for publication, manuscript ID: CC-COM-10-2017-007806 (2017).

4. T. Vasiliu, C. Cojocaru, A. Rotaru, G. Pricope, M. Pinteala, L. Clima. Optimization of Polyplex Formation between DNA Oligonucleotide and Poly(L-Lysine): Experimental Study and Modeling Approach. *Int. J. Mol. Sci*., 18, 1291, (2017).
   DOI: 10.3390/ijms18061291

5. E. L. Ursu, F. Doroftei, D. Peptanariu, M. Pinteala, A. Rotaru*. DNA-assisted decoration of single-walled carbon nanotubes with gold nanoparticles for applications in surface-enhanced Raman scattering imaging of cells. *J. Nanopart. Res*., 19, 181, (2017).
   DOI: 10.1007/s11051-017-3876-9

6. N. L. Marangoci, L. Popovici, E. L. Ursu, R.Danac, L. Clima, C. Cojocaru, A. Coroaba, A. Neamtu, I. Mangalagiu, M. Pinteala, A. Rotaru*. Pyridyl-indolizine derivatives as DNA binders and pH-sensitive fluorescent dyes. *Tetrahedron*, 50, 8215–8222, (2016).
   DOI: dx.doi.org/10.1016/j.tet.2016.10.052

International Meetings

1. **Alexandru Rotaru, "**Supramolecular systems for biomedical applications". 1st International Workshop "PROTEOMICS – from Introduction to Clinical Applications", July 9-13, Iasi, Romania. **(30 min. Oral Presentation)**

2. **Alexandru Rotaru, "**Cell Imaging: from new non-toxic Fluorescent Dyes to Raman Probes based on Metal Nanoparticles – Carbon Nanotube Nanoconjugates". 9th Cristofor I. Simionescu Symposium Frontiers in Macromolecular and Supramolecular Science, June 13-14, 2017, Iasi, Romania. **(30 min. Oral Presentation)**

3. **Alexandru Rotaru** "DNA-Assisted Decoration of Single-Walled Carbon Nanotubes with Metal Nanoparticles". 20th Romanian International Conference on Chemistry and Chemical Engineering (RICCCE-2017), September 6 – 9, 2017, Poiana Brasov, Romania. **(15 min. Oral Presentation)**

4. **G. Pricope, D. Peptanariu, A. Rotaru, M. Pinteala and M. Barboiu.** Flexible Guanosine-Based Hydrogels for Biomedical Applications. *12th International Conference on Colloid and Surface Chemistry (ICCSC),* 16.05. – 18.05. 2016, Iasi, Romania. (**Poster**)

5. **E. L. Ursu and A. Rotaru.** DNA–gold nanoparticle–single-walled carbon nanotubes hybrids for biomedical applications, *XIIth French-Romanian Polymer Meeting*, 05.09. – 07.09.2016**,** Sophia Antipolis, France. (**Poster**)

6. **N. L. Marangoci and A. Rotaru.** Fluorescence behaviour and DNA binding affinity studies of new pyridyl-indolizine derivatives. *XXXIV-th Romanian Chemistry Conference,* 04.10. – 07.10.2016, Calimanesti-Caciulata, Valcea, Romania. (**Poster**)

7. **A. Dascalu, E-L. Ursu, F. Doroftei, N. Marangoci and A. Rotaru.** DNA assisted functionalization of gold nanoparticles with cyclodextrin moiety. *"Alexandru Ioan Cuza" University Days*, 27.10. – 28.10.2016, Iasi, Romania. (**Poster**)

8. **L. Popovici, N.-L. Marangoci, R. Danac, C. Cojocaru, I. Mangalagiu, A. Rotaru.** Pyridyl-indolizine derivatives as DNA binders and pH-sensible fluorescent dyes. *"Alexandru Ioan Cuza" University Days*, 27.10. – 28.10.2016, Iasi, Romania. (**Poster**)

9. **Alexandru Rotaru.** Design, assembly and visualization by AFM of chemical modifications on DNA origami nano-structures. *International Workshop. Biomolecular nanostructures for the study of biophysical and biochemical processes*. 08-09.10.2015, Potsdam, Germany. (**Presentation 30 min**)

10. **Elena-Laura Ursu, Alexandru Rotaru.** DNA-Mediated Gold Nanoparticle Decoration of Dispersed Single-Walled Carbon Nanotubes for Applications in Theranostic. *SFNano European Nanomedicine Meeting*, 07-09.12.2015, Grenoble, France. (**Poster**)